Available online at www.sciencedirect.com
SCIENCE DIRECT
Wear 260 (2006) 1317–1323
WEAR
www.elsevier.com/locate/wear

The influence of material build up around artificial defects on rolling contact fatigue life and failure mechanism

R.C. Dommarco [a,*], P.C. Bastias [b], C.A. Rubin [c], G.T. Hahn [c]

[a] *Grupo Tribología, Fac. Ing., UNMdP, B7608FDQ, Mar del Plata, Argentina*
[b] *DANA Corporation, Sealing Products, 100 Plumley Drive, Paris, TN 38242, USA*
[c] *Mechanical Engineering Department, Vanderbilt University, Nashville, TN 37235, USA*

Received 22 April 2005; received in revised form 13 September 2005; accepted 21 September 2005
Available online 24 October 2005

Abstract

This paper reports the results obtained in tests conducted to evaluate the evolution of wear tracks and artificial defects under rolling contact fatigue (RCF) loading and its effect on RCF life. The experiments were conducted on specimens of different materials commonly used in rolling bearings and gears. The artificial defects were introduced with the rounded tip of a Rockwell-C type indenter, with a diameter of ∼120 μm. The evolution of the micro-roughness profiles was followed, in the rolling and transversal directions, for both, artificial defect and wear track. The RCF lives of the samples were correlated with the build up height. Furthermore, the RCF lives of three variants of the SAE 52100 steel with artificial defects were compared to those obtained for the same variants where the build ups had been machined off. In the later case, the lives were observed to increased by a factor close to two; while the spall appearance remained unchanged indicating a similar failure mechanism. These results give room to question the precision and validity of finite element models, when analyzing artificial defects without proper accounting for the build up, i.e. surface roughness, and subsequent life theories formulated to match the numerical results. This paper also deals with the influence of artificial defects (when used to accelerate tests) on the life reduction factor for different materials, which was observed to be dependent on the material hardness.
© 2005 Elsevier B.V. All rights reserved.

Keywords: Contact fatigue life; Artificial defect; Build up; Profile evolution; Failure mechanism

1. Introduction

Crack nucleation under cyclic loading conditions in steel is controlled by the presence of metallic and non-metallic inclusions and geometric discontinuities, either in bending fatigue [1,2] or rolling contact fatigue (RCF) [3]. It is well known that fatigue failure in bending typically originates at the external fibers, where the most unfavorable stresses and strains actuate.

The RCF failure, under ideal working conditions, i.e. when $\lambda > 3$ (where λ is the ratio of the minimum oil film thickness to the compound surface roughness) originates in the subsurface region, in coincidence with the most unfavorable strains and stresses. In this case, metallurgical defects work as stress raisers, which lead to crack nucleation and, then, propagation. It has been demonstrated [3] that even small inclusions, i.e. ∼2–4 μm, may lead to failure, even though this also depends on material properties and residual stresses [4]. Under low to moderate load conditions, the surface irregularities (roughness) may be tolerated and accommodated by the lubricant film thickness.

With the advent of modern steel manufacturing technologies (cleaner steels) and the requirement of higher mechanical solicitations, leading to thinner oil films, i.e. $\lambda < 2$, the failure mode has shifted from a subsurface, to a surface-dominated one. The RCF failure is now found to be controlled by the characteristics of the contacting surfaces, i.e. the size, morphology and orientation of the micro asperities and the presence of grinding marks or indentations [4–6]. The surface irregularities present in the contact area may produce large local perturbations of the Hertzian pressure distribution in the form of narrow, stationary pressure spikes. Some computational models have shown that discontinuities as small as 5 μm deep may produce stress spikes that double the maximum Hertz stress considering elastic conditions [7–9].

* Corresponding author. Tel.: +54 223 481 6600x245; fax: +54 223 481 0046.
E-mail address: dommarco@fi.mdp.edu.ar (R.C. Dommarco).

0043-1648/$ – see front matter © 2005 Elsevier B.V. All rights reserved.
doi:10.1016/j.wear.2005.09.009

Researchers are focused these days on the surface nucleation phenomena. Accelerated tests, which may include the use of high loads, high roughness, debris in oil, or artificial defects placed on the wear tracks have become a standard practice. Among the most commonly used artificial defects, hemispherical dents or furrows are found, particularly the former because of their similarity with actual indentations produced in a machine with contaminated oil.

Numerical models are often used to evaluate the effect of an artificial defect on the strain and stress fields at or near the defect, and then are correlated to the RCF lives in order to obtain empirical theories capable of predicting life. Simplified plane strain (2D) finite element analyses considered an ellipsoidal indentation with its longer radius perpendicular to the rolling direction. Many times, however, these simplified models neglect to account for the presence of a build up (BU) around the natural defects (produced by debris in the oil) or artificial defect's [9–11]. Also in an experimental study [12] build up free artificial defects were obtained by electric discharge machining.

Other analytical and 2D numerical studies considering the influence of the artificial defect's build up under rolling contact loading [13–15] or pure sliding contact [16] show that the perturbation of the contact pressure produces pressure spikes up to 3–4 times higher than p_0.

Even models without a build up [8] show that the maximum equivalent stresses (von Mises) take place at the edges, when the contacting cylinder is positioned directly over the artificial defect. It was found [17] that the cyclic plasticity and residual stresses are higher at the trailing edge of the groove, where the spalls are seen to nucleate. This gave rise to the speculation that the build up should considerably modify the strain and stress fields near the surface and, thus, plays a more important role in crack nucleation than suspected.

To the best of the author's knowledge the effects of artificial defect's build up on the RCF life was not experimentally studied before. Therefore, different steel variants were evaluated by introducing artificial defects, and their RCF lives compared to the ones obtained for samples where the artificial defects build up's had been previously machined off. The failure mechanism was also studied by following the artificial defect's profile evolution in the rolling and transversal direction for both the unshaved and the shaved specimens. The influence of the artificial defects on the life reduction factor was also evaluated.

2. Experimental procedure

2.1. Rolling contact fatigue tests

The RCF tests were carried out with a "ball-rod rolling contact fatigue tester" [18]. The present study was conducted using a previously described modification of this experimental set up [19]. The sample rotates at 3600 rpm and the lubrication feed was 8–10 drops per minute of Exxon 2380 turbo oil at an operating temperature of 70 °C. The experiment uses SAE 52100 steel balls with a roughness of 0.11 μm. These "rough balls" were provided by NTN Bower. The experimental conditions for the RCF tests lead to a minimum oil film thickness, $h_0 = 0.17$ μm, as calculated by using the equation proposed by Hamrock and Dowson [20].

The load applied during the experiment was chosen to produce a $p_0/k_k = 6$, where p_0 is the maximum Hertz stress and k_k is the kinematic yield strength for the material. This implies that the tests were carried out over the shakedown limit. For the steel samples k_k was equal to 600 MPa and thus $p_0 = 3.6$ GPa. For the ADI samples, on the other hand, k_k was determined to be 450 MPa and thus a $p_0 = 2.7$ GPa was used, According to hertzian (elastic) theory these pressures produce an elliptical contact patch in steel samples with minor (circumferential or rolling direction) and major (axial direction) contact lengths equal to: $2a \approx 313$ μm, and $2b \approx 549$ μm, respectively. The minor and major contact widths for the ADI were $2a \approx 0.265$ mm and $2b \approx 0.465$ mm, respectively.

The fatigue tests results were analyzed using the two-parameter Weibull statistics and the ten (L_{10}), fifty (L_{50}) and medium (η, at 63.3% failure probability) lives were evaluated. The number of tests carried out per sample variant is listed in Table 2. The rolling direction was defined as opposite to the direction of sample rotation.

2.2. Sample preparation

The samples were made out of one variant of AISI 440C steel, five variants of SAE 52100 and one variant of austempered ductile iron (ADI). Table 1 lists sample definitions, heat treatment parameters and hardness values.

The sample shape favors its manipulation and the use of the hardness tester to introduce small artificial defects. The specimens were mounted in the RCF test rig and rolled over during 35–40 min in order to create a wear track over which the artificial defects were placed. The tests were then continued until evidence of the spall formation was detected by the associated increase in the vibration level and the machine automatically stopped.

The same degree of penetration of the diamond rounded tip of a Rockwell C indenter was used for all samples, in order to obtain hemispherical artificial defects with ~120 μm in diameter and ~6 μm in depth. Specimens of variants, RI, RII and RIII were carefully and manually polished ("shaving") to eliminate the build ups around the hardness indentations (RI-NB, RII-NB and RIII-NB). The shaving process used assures that

Table 1
Material treatments and hardness for all variants tested

Sample ID	Treatment	Hardness HRC ($Knoop_{500}$)
RI	Martensitic hard. + temp. at 160 °C/1.5 h	62.5
RII	Martensitic hard. + temp. at 200 °C/1.5 h	60.5
RIII	Martensitic hard. + temp. at 240 °C/1.5 h	58.5
A1	Martensitic hard. + carbonitriding to ~50 μm	65 (850)
AC2	Martensitic hard. + carbonitriding to ~100 μm	66 (880)
440 C	Martensitic hard. + temp	60.5
ADI	Austempered at 240 °C/1 h	45

Specimens RI through AC2 were made of SAE 52100.

the material structure was not affected. The analysis of the artificial defect's profiles after shaving proved that the diameter and depth remained unchanged.

Profiles measurements were made with a Talysurf 10 profilometer along two different directions: parallel with respect to the wear track or rolling direction and perpendicular with respect to the wear track, i.e. along the sample axial direction. Profile data acquisition was made through a computer and then plotted. Data from the rolling direction was mathematically converted into a flat profile.

The hardness was measured using the Rockwell C (HRC) method for the quenched and tempered, and austempered samples and the Knoop hardness with 500 g (HK_{500}) for the carbonitreded samples.

3. Results and discussion

3.1. Rolling contact fatigue tests

The artificial defect's profile measurements show that an hemispherical dent with a diameter of ~120 μm and ~6 μm deep is accompanied by a small build up formation about 0.4–0.9 μm height, which was either not detected or reported by studies conducted using optical or electron microscopes. The sample profiles across the wear track and artificial defect for all steel variants are shown in Fig. 1, including the profile for the shaved RII sample (RII-NB). The characteristic dimensions of the artificial defects, i.e. diameter, depth and BU height, for all the material variants are shown in Fig. 2.

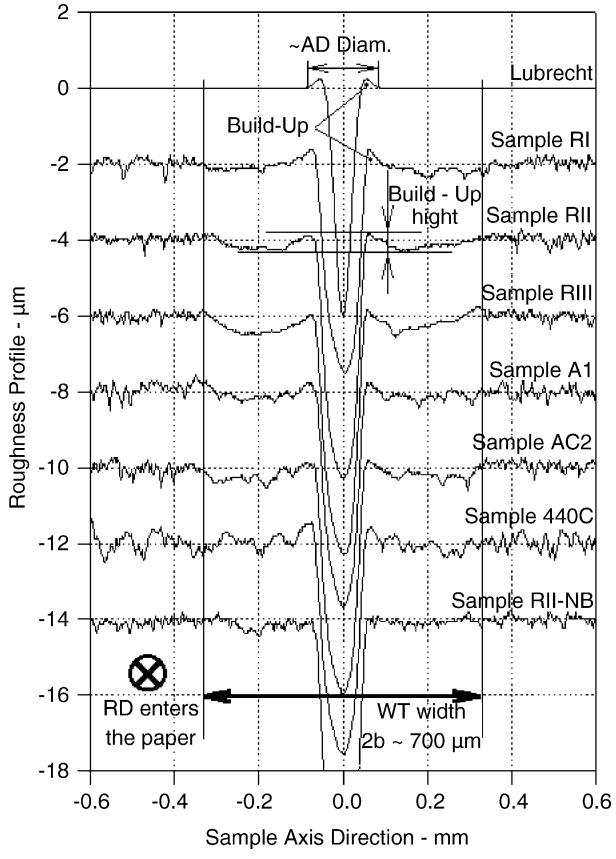

Fig. 1. Artificial defect and wear track profile obtained for the different samples tested. Also included is the RII sample with machined off BU (RII-NB). Lubrecht profile is from Lubrecht et al. (1992).

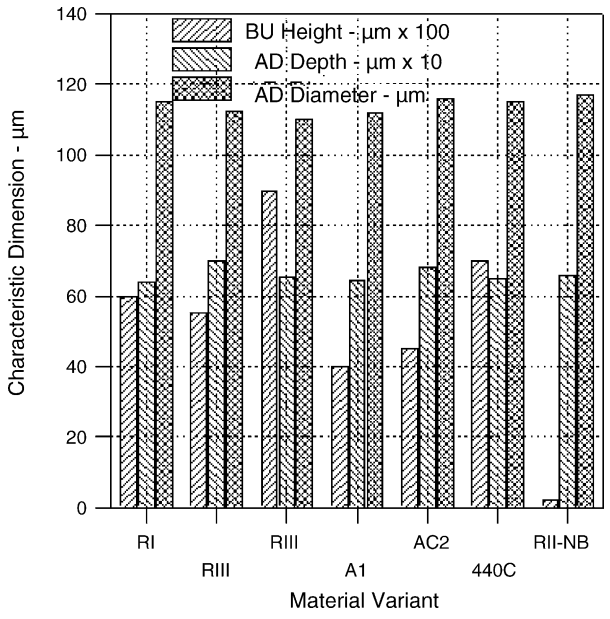

Fig. 2. Artificial defect (AD) characteristic dimensions: diameter, depth and build up height, obtained for the tested samples. Refer to Table 1 for sample definitions.

Table 2 summarizes the RCF test results, showing the characteristic Weibull parameters, i.e. L_{10}, L_{50} and η lives. Fig. 3 shows the correlation obtained for build up height and L_{10} and L_{50} lives for each steel variant. RCF lives appear to be strongly dependent on build up height, particularly L_{50} life, while diameter and depth of the artificial defect were kept unchanged.

The procedure used to place the artificial defects on the wear track, assures that the diameter and depth obtained will be the same for all the different samples. Therefore, different build up height will be connected in some way with material response to plasticity. In order to shed light about the build up's influence on

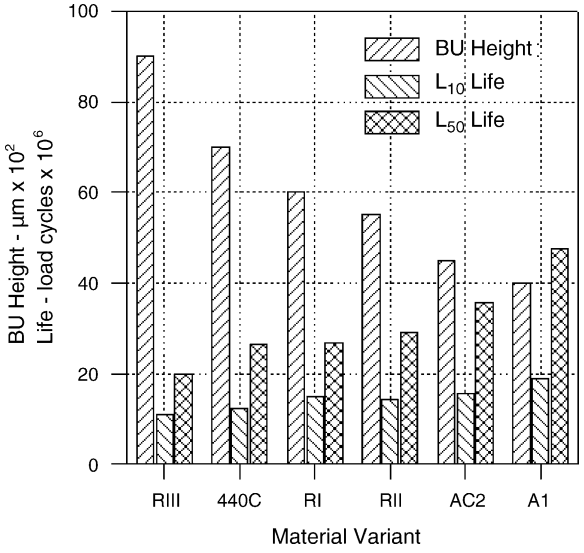

Fig. 3. Rolling contact fatigue resistance, L_{10} and L_{50} lives, correlated to build up height for samples with treatments and hardness as listed in Table 1.

Table 2
Rolling contact fatigue lives

Sample	Number of tests	Life ($\times 10^6$ cycles)			Weibull slope, β	Correl. factor, r	Determ. coef., r^2
		L_{10}	L_{50}	Characteristic life, η			
440C	16	12.20	26.57	26.57	2.891	0.921	0.849
RI	10	14.98	26.90	29.71	3.272	0.959	0.919
RI-NB	6	34.67	55.97	61.44	3.933	0.797	0.635
RII	10	14.10	29.17	33.92	2.553	0.928	0.862
RII-NB	6	29.92	58.18	66.22	2.833	0.959	0.920
RIII	10	10.93	20.00	22.17	3.221	0.982	0.963
RIII-NB	6	9.92	20.87	24.12	2.535	0.974	0.949
A1	10	18.75	47.46	56.85	2.029	0.890	0.791
AC2	10	15.43	35.59	41.88	2.255	0.979	0.959
ADI	8	2.25	3.14	3.34	5.680	0.946	0.895

Characteristic life, η corresponds to a failure probability of 63.2%. Variants tested with out artificial defects.

RCF life, two steel variants (RI and RII) were specially prepared, by the introduction of artificial defects and subsequent mechanical shaving of their build ups. The effectiveness of shaving was controlled by using a profilometer and checking that the artificial defect diameter and depth remained the same after shaving (Fig. 1, sample RII-NB)

The results obtained on shaved samples have shown a dramatic increase in the RCF life, confirming the strong influence of the build up on the RCF life. As listed in Table 2, lives obtained for sample RI without build up (RI-NB) and sample RII without build up (RII-NB) were doubled with respect to RI and RII samples, respectively. The results obtained for the RIII-NB sample were different and will be discussed later. Therefore, when the build up's were removed by shaving (zero height), the RCF lives increased by a factor close to 2 while the failure appearance remained unchanged.

3.2. Failure mechanism

The failure appears in the form of a spall at the artificial defect's trailing edge, having the characteristic V-shape pointing opposite with respect to the RD, Fig. 4, and having a transversal dimension limited by the wear track width. Typical angles for crack propagation with respect to the wear track were measured to be in the range of 16–32°. Optical observation may lead to the conclusion that the spall nucleates besides the artificial defect, but it was demonstrated earlier [19] that spall nucleation actually takes place not outside but inside the limits of the artificial defect, as shown in Fig. 5b.

The localized plastic deformation responsible for spall nucleation taking place all around the AD, is increased by the presence of the build up. Nevertheless, it was observed that 100% of failures originate at the artificial defect's trailing edge (region IV of Fig. 5a), in coincidence with the analyses [8,17] indicating that the maximum equivalent stress (von Mises) takes place in this region. Furthermore, finite element analysis and laboratory tests have shown that the rolling contact loading may produce small forward material flow on the wear track. This complex forward ratcheting is evidence of continued plastic deformation due to tangential forces originating from a combination of elastic deformations and friction forces at the contact. It was hypothesized that forward flow would increase locally when the build up is present, as the geometry of the contact changes and a horizontal force component arises. In order to ascertain the deformation during rolling, the artificial defect profiles evolution were followed as a function of the number of load cycles.

The artificial defect overrolling progressively deforms the build up until it has completely disappeared. The severity of plastic deformation varies when considering different build up regions as defined in Fig. 5a. Material from region I, when rolled over, is deformed forward (in the rolling direction) and forced to enter the artificial defect crater. A similar process takes place

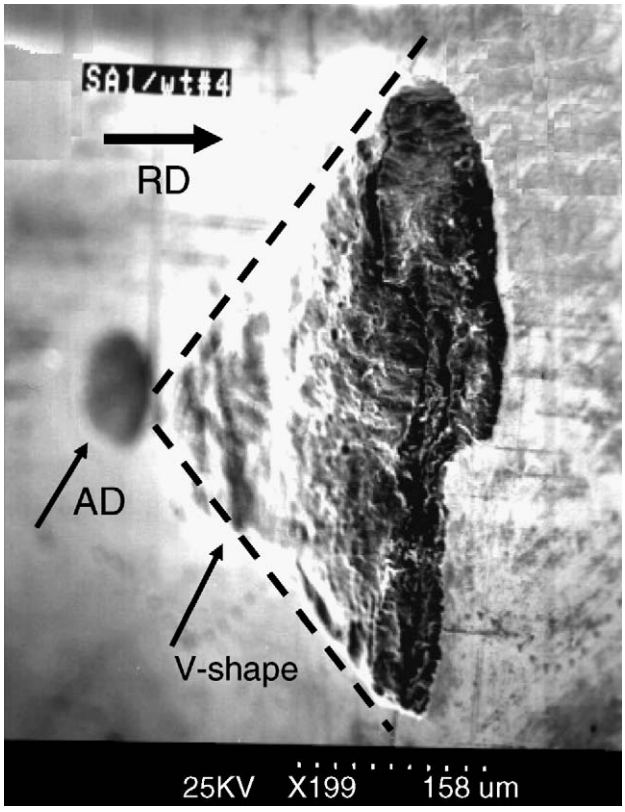

Fig. 4. V-shaped spall nucleated at the artificial defect trailing edge pointing opposite with respect to the RD. Transversal dimension is limited by the wear track width.

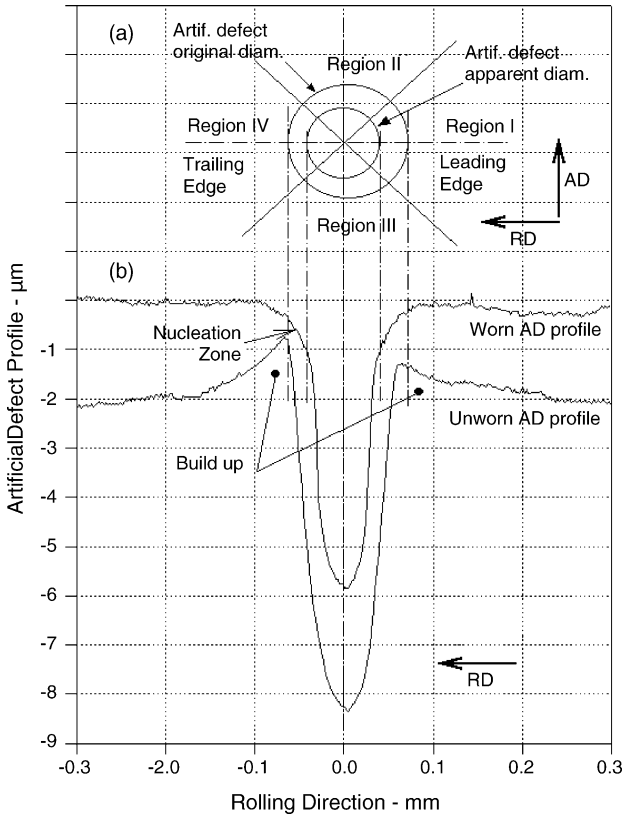

Fig. 5. Artificial defect and spall nucleation zone. (a) Artificial defect view defining regions I, II, III and IV; leading and trailing edges. (b) Artificial defect profile for the as new and used conditions. Nucleation zone as determined in Ref. [19]. RD, rolling direction, AD, axial direction.

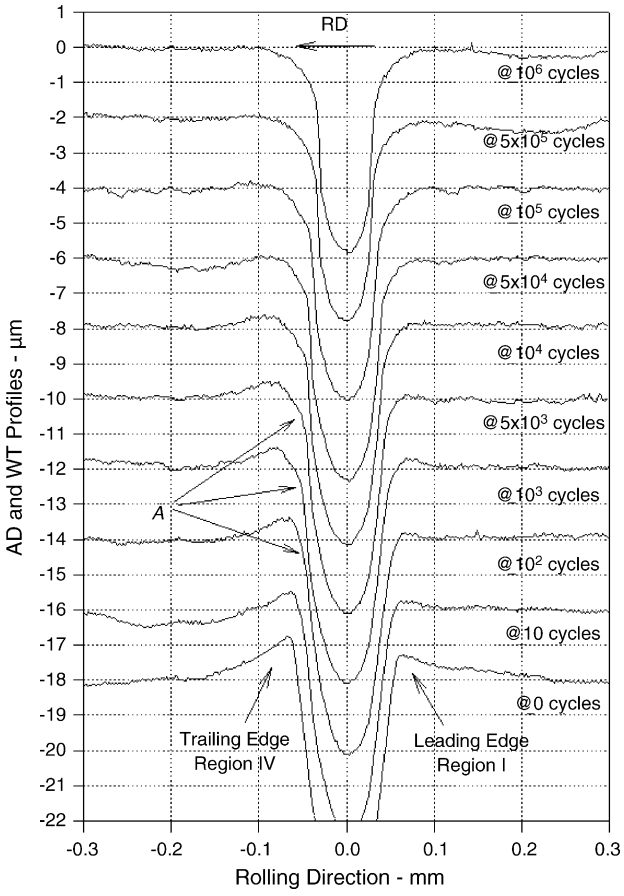

Fig. 6. Artificial defect profile evolution as a function of the number of stress cycles in the rolling direction (RD). Sample RII with build up.

in regions II and III, where the build up is also forced to enter the crater. In region IV the build up is also displaced forward. In this region, however, there is no crater ahead of the material to facilitate its deformation. Furthermore, ball vertical movement is constrained by the outer ring of the testing machine, thus leading to a heavier plastic deformation.

The artificial defect profile evolution is an experimental evidence of the phenomena described above and it was followed as a function of the number of load cycles in both, the rolling and axial directions. The evolution, shown in Fig. 6, reveals that the artificial defect profile changes after a relatively small number of loading cycles. The most critical topological change appears to take place at the build up, as its height in the trailing edge (region IV) is reduced to a half of its initial value after 10 load cycles and almost disappears after 1×10^4 cycles, i.e. less than 0.05% of the total life to failure. On the other hand, the build up in the leading edge (region I) is almost completely displaced in just 1×10^3 load cycles. This difference in the number of cycles necessary by the different build up regions to disappear may be related to the facility encountered by the rolling elements (in this case the balls) to displace material forward.

The profile evolution along the axial direction, Fig. 7, shows the manner in which the build up from regions II and III is forced to enter the artificial defect crater and progressively reducing its apparent diameter [19], as seen by optical microscopy due to the reflection angle of light. This is also shown in Fig. 5a, besides the original diameter. Moreover, there is a gradual loss of symmetry when looking the profiles obtained along the rolling direction, due to the fact that mainly the material from region I is displaced into the indentation, Fig. 6.

When the ball is directly over the artificial defect, the contact area is ring shaped, with the inner diameter of the contact area being subjected to different stress conditions depending on the region being considered. It should be taken into account that the profiles shown in Figs. 6 and 7 were measured in the unloaded condition as the elastic deformation makes points located under the surface level to get in contact under load. Since the stress condition will be related to the forward flow phenomena, material at the contact area internal diameter, in region I, is subjected to compression while at the equivalent point of region IV will be in traction. The result can be appreciated in Fig. 8 where traction forces at the trailing edge have produced the opening of the crack mouth, in agreement with previous finite element analysis predicting higher equivalent stresses at the trailing edge or region IV [17,21] (see also Fig. 5 to locate the crack position).

The presence of the build up increase the amount of material to be accommodated by the mechanism described above and, thus, increasing plasticity and reducing the time required to reach the critical deformation needed at the artificial defect trailing edge for crack nucleation. Therefore, by shaving the build up, plastic deformation at region IV or the trailing edge is reduced

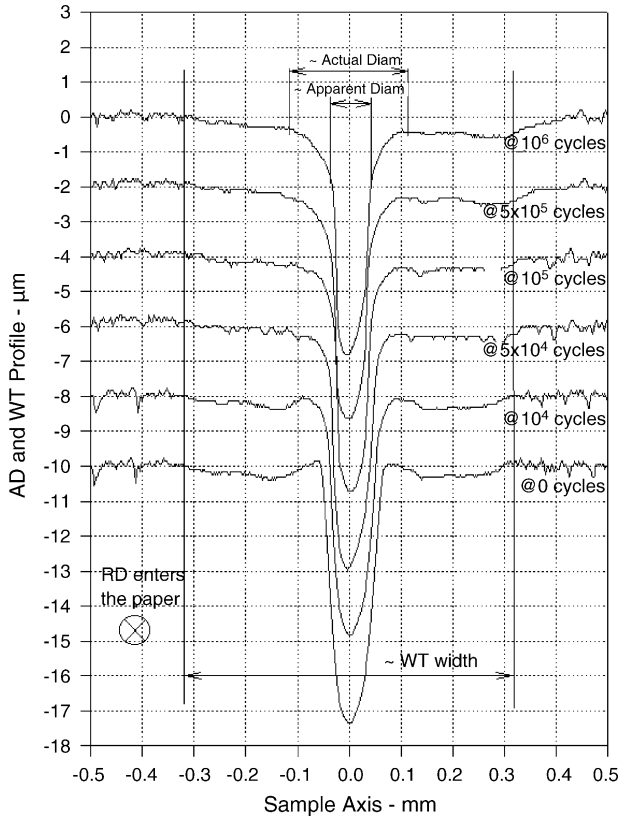

Fig. 7. Artificial defect profile evolution as a function of the number of stress cycles perpendicular to the rolling direction. Sample RII with build up.

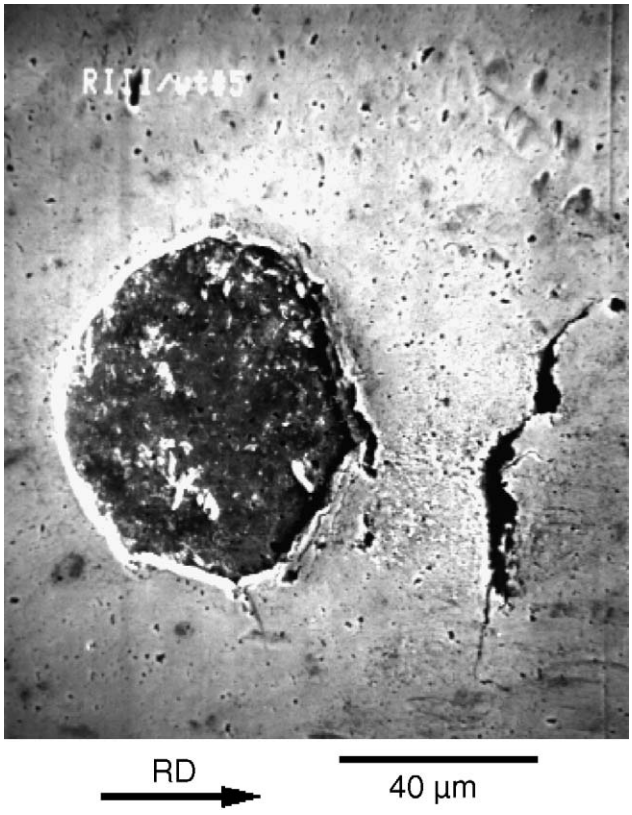

Fig. 8. Nucleated crack over the artificial defect trailing edge (region IV) in RIII at 10.4×10^6 cycles, showing crack mouth opening due to traction forces.

in such amount that the number of stress cycles needed for crack nucleation and propagation, i.e. the RCF life, doubles.

3.3. Life reduction factor using artificial defects

The explanation, on how a relatively small build up has so much stronger effect than the rest of the artificial defect's characteristics on the RCF life, does not explain, however, why RIII and RIII-NB lives were basically the same. In this respect it should be pointed out that general degradation of the wear track took place for the RIII samples, far from the artificial defects, leading to the formation of many randomly distributed spalls. This shows a low sensitivity of the RIII steel variant to the presence of the artificial defects. The same effect was observed on ADI's samples proving to be completely insensitive to the introduction of artificial defects [22].

The presence of the artificial defects reduces the RCF life to failure of the samples by a factor whose value depends on the material variant being tested. The analysis of the RCF lives obtained in the present paper, for the different material variants, indicates that the life reduction factor depends on sample hardness. Fig. 9 shows the results for tests run with and without artificial defects. The life reduction factor was higher than 3 for the carbonitreded specimens A1 and AC2, while on the other end was 1.6 for RIII and 1 for ADI variants. It should be taken into account that the ADI variant has graphite nodules, which in some way work as natural defects. Relatively low hardness quenched SAE 4140 steel tempered at a hardness level of 50 HRC has also shown a life reduction factor of 1 [23], even when tested in a different RCF test rig but at a similar p_0/k_k relation. Therefore, relative low hardness materials appear to be insensitive to the use of artificial defect when large plastic deformations are involved. This point is of significance when evaluating different material or heat treatments for a given application by accelerated tests of any type. If a longer RCF life is obtained in a harder material, an

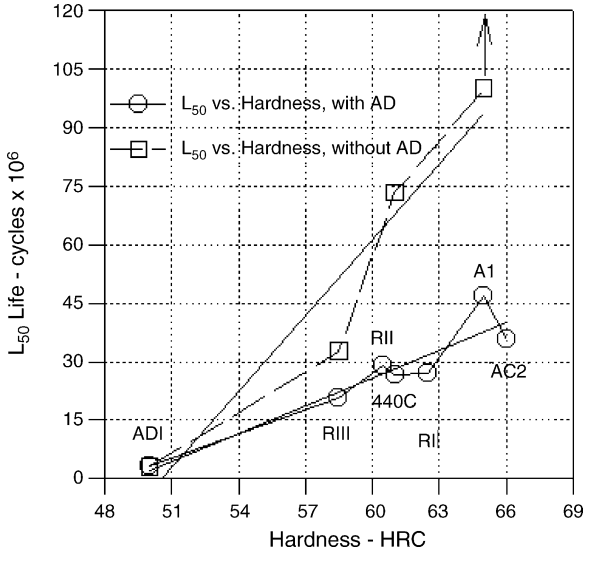

Fig. 9. Rolling contact fatigue lives for specimens with and without artificial defects (AD). RCF tests for A1 samples with out artificial defects suspended with out failure after 10^8 loading cycles.

even greater difference should be expected for a test conducted under ideal conditions.

4. Conclusions

The BU formed at the edge of the artificial defects strongly affects the life to failure under rolling contact loading. It was observed by following the artificial defect's profile evolution that, even though the build up is very small (less than 1 μm height), it strongly affects the RCF life by increasing micro-plasticity at the artificial defect's trailing edge. This observation was corroborated by evaluating samples with the artificial defect build ups shaved, where the life to failure was doubled with respect to the life for non-shaved build ups. This experimental results are valuable as reference values for numerical models. It was demonstrated that the life reduction factor of artificial defects varies with the mechanical properties of the samples.

References

[1] A. Melander, M. Rolfsson, A. Nordgren, B. Jansson, H. Hedberg, T. Lund, Influence of inclusion contents on fatigue properties of SAE 52100 bearing steels, Scand. J. Metall. 20 (1991) 229–244.
[2] Y. Murakami, M. Endo, Effect of defects, inclusions and in homogenities on fatigue strength, Fatigue 16 (1994) 163–182.
[3] Q. Chen, E. Shao, D. Zhao, J. Guo, Z. Fan, Measurement of critical size of inclusions initiating contact fatigue cracks and its application in bearing steel, Wear 147 (1991) 285–294.
[4] K. Böhm, H. Schlicht, O. Zwirlein, R. Eberhard, Non-metallic inclusions and rolling contact fatigue, ASTM STP 575, ASTM, 1975. pp.96–113.
[5] H. Lorosch, Influence of load on the magnitude of the life exponent for rolling bearings, in: J.J.C. Hoo (Ed.), Rolling Contact Fatigue Testing of Bearing Steels, ASTM STP 771, 1982, pp. 275–292.
[6] Ch.A. Moyer, Power density development: the role of improved line contact performance, AGMA Technical Paper, 89 FTM 3, 1989.
[7] P.C. Bastias, V. Bhargava, A. Bower, J. Du, V. Gupta, G.T. Hahn, S. Kulkarni, A. Kumar, X. Leng, C.A. Rubin, Analysis of rolling contact spall life in 440C steel bearing rims, NASA Report NAS8-37764, 1991.
[8] P.C. Bastias, G.T. Hahn, C.A. Rubin, V. Gupta, X. Leng, Analysis of rolling contact spall life in 440C bearing steel, Wear 171 (1994) 169–178.
[9] V. Gupta, P.C. Bastias, G.T. Hahn, C.A. Rubin, Influence of indent geometry on repeated two-dimensional rolling contact, J. Tribol. 117 (1995) 655–659.
[10] J.M. De Mul, J.M. Vree, J.C. Kuypers, The influence of certain raceway dent geometries (3D) on contact stresses and rating fatigue life of rolling bearings, J. Tribol. 109 (1987) 452–461.
[11] J. Zhao, F. Sadeghi, H.M. Nixon, A finite analysis of surface pocket effects in hertzian line contact, J. Tribol. 122 (2000) 47–54.
[12] W. Cheng, H.S. Cheng, L.M. Keer, X. Ai, Surface crack initiation under contact fatigue: experimental observation and contact analysis, J. Tribol. 115 (1993) 658–665.
[13] W. Holzhauer, Surface changes around large raceway indentations during run-in of tapered roller bearings, Tribol. Transact. 34 (3) (1991) 361–368.
[14] A.A. Lubrecht, R.S. Dwyer-Joyce, E. Ionnides, Analysis of the influence of indentations on contact life, in: D. Dowson, et al. (Eds.), Wear Particles, Elsevier Science Publishers B.V., 1992, pp. 173–181.
[15] D. Nélias, F. Ville, Detrimental effects of debris dents on rolling contact fatigue, J. Tribol. 122 (2000) 55–64.
[16] S. Coulon, I. Jubault, A.A. Lubrecht, F. Ville, P. Vergne, Pressure profiles measured within lubricated contacts in presence of dented surfaces. Comparison with numerical models, Tribol. Int. 37 (2004) 111–117.
[17] V. Gupta, Study of the effects of surface irregularities in rolling contact performance, PhD Thesis Dissert, Vanderbilt University, Nashville, TN, USA, 1994.
[18] D. Glover, in: J.J.C. Hoo (Ed.), A Ball-rod Rolling Contact Fatigue Tester, ASTM STP-771, 1982, pp. 107–124.
[19] R.C. Dommarco, P.C. Bastias, G.T. Hahn, C.A. Rubin, The use of artificial defects in the 5-ball-rod rolling contact fatigue experiments, Wear 252 (2002) 430–437.
[20] B.J. Hamrock, D. Dowson, Isothermal elastohydrodynamic lubrication of point contacts. Part III Fully flooded results, J. Lubric. Technol. (Trans. ASME) 99 (1977) 264–276.
[21] M.B. Howell, C.A. Rubin, G.T. Hahn, The effect of dent size on the pressure distribution and failure location in dry point frictionless rolling contacts, J. Tribol. 126 (2004) 413–421.
[22] R.C. Dommarco, P.C. Bastias, H.A. DallíO, G.T. Hahn, C.A. Rubin, Rolling contact fatigue resistance of austempered ductile iron, Wear 221 (1998) 69–74.
[23] R.C. Dommarco, J.D. Salvande, Contact fatigue resistance of austempered and partially chilled ductile iron, Wear 254 (2003) 230–236.